Sediment patterns near a model patch of reedy emergent vegetation

Citation: Follett, Elizabeth M., and Heidi M. Nepf. "Sediment Patterns Near a Model Patch of Reedy Emergent Vegetation." Geomorphology 179 (December 2012): 141–151.

As Published: http://dx.doi.org/10.1016/j.geomorph.2012.08.006

Publisher: Elsevier

Persistent URL: http://hdl.handle.net/1721.1/99230

Version: Author's final manuscript: final author's manuscript post peer review, without publisher's formatting or copy editing

Sediment patterns near a model patch of reedy emergent vegetation

Elizabeth M. Follett* and Heidi M. Nepf[1]

Department of Civil and Environmental Engineering, Massachusetts Institute of Technology, MIT Bldg. 48-216, 77 Massachusetts Avenue, Cambridge, MA 02139, USA

*Corresponding author. Tel.: +1 (847) 471-8878, Fax: +1 (817) 258-8850, E-mail: emf@mit.edu.

[1]E-mail: hmnepf@mit.edu.

Abstract

This laboratory study describes the sediment patterns formed in a sand bed around circular patches of rigid vertical cylinders, representing a patch of reedy emergent vegetation. The patch diameter was much smaller than the channel width. Two patch densities (solid volume fraction 3% and 10%) and two patch diameters (22 and 10 cm) were considered. For flows above the threshold of sediment motion, patterns of sediment erosion and deposition were observed around and within the patch. Scouring within the patch was positively correlated with turbulent kinetic energy in the patch. For sparse patches, sediment scoured from within the patch was mostly deposited within one patch diameter downstream of the patch. For dense patches, which experience greater flow diversion, sediment scoured from the patch was carried farther downstream before deposition along the patch centerline. Differences between the sparse and dense patch patterns of deposition are explained in the context of flow diversion and wake structure, which are related to a nondimensional flow blockage parameter. While sediment was redistributed near the patch, observations suggest that net deposition was not recorded at the reach scale.

Keywords: emergent vegetation; sediment transport; wake; deposition; flume; porous patch

Abbreviations: (SAFL) Saint Anthony Falls Laboratory; (TKE) turbulent kinetic energy

1. Introduction

Vegetation can increase flow resistance and reduce flow conveyance so that many consider it a nuisance in culverts and stream channels (Kouwen and Unny, 1975). However, vegetation improves water quality by removing nutrients from and releasing oxygen to the water column (Chambers and Prepas,1994; Wilcock et al., 1999; Schulz et al., 2003). It also promotes habitat diversity by creating a diversity of flow regimes (Crowder and Diplas, 2000; Kemp et al., 2000; Crowder and Diplas, 2002). The bed stabilization effects of vegetation have been widely recognized (Wynn and Mostaghimi, 2006; Afzalimehr and Dey, 2009; Wang et al., 2009; Li and Millar, 2010; Pollen-Bankhead and Simon, 2010). As an example, vegetation has been shown to stabilize both single thread (Tal and Paola, 2007) and meandering (Braudrick et al., 2009) channel morphologies. Sediment loading from bank erosion is also diminished by vegetation (Lawler, 2008). The reduction of velocity within vegetated regions can encourage deposition of fine particles and sediment retention (Abt et al., 1994; Lopez and Garcia, 1998; Cotton et al., 2006; Gurnell et al., 2006) and promote the growth of ridges and islands (Edwards et al., 1999; Tooth and Nanson, 1999; Gurnell et al., 2001, 2008). Similarly, aeolian literature reports that vegetation accelerates the nucleation of dunes (Luna et al., 2011). While most studies have focused on enhanced deposition within vegetated regions, vegetation also promotes erosion under some conditions. Specifically, close to vegetated regions of finite width, the diversion of flow away from the vegetation leads to the acceleration of flow along the vegetation edge, which causes localized erosion (Fonseca et al., 1983;

Bouma et al., 2007; Bennett et al., 2008; Rominger et al., 2010).

Recognizing the benefits of vegetation to river health, ecologically minded management and replanting of denuded regions are now encouraged (Mars et al., 1999; Pollen and Simon, 2005). However, successful river restoration requires an understanding of how vegetation impacts flow and sediment transport. For example, Larsen and Harvey (2011) explained the stability of different landscape patterns in the Everglades by coupling vegetation dynamics to both sediment transport and flow. While many studies have described long, uniform reaches of vegetation, only a few have considered finite patches of vegetation. Bennett et al. (2002, 2008) described how the introduction of finite patches along the wall of a channel changes the flow and erosion pattern. The channel response was found to depend on both the shape and density of the rigid model stems. In particular, alternating patches of semicircular shape were recommended to promote the restoration of meandering geometries.

In this study we consider the erosion pattern associated with a circular patch of emergent vegetation located at mid-channel, making connections to flow structure previously described by Zong and Nepf (2012). Zong and Nepf considered circular arrays of diameter D constructed from circular cylinders, each of diameter d, at a density of n cylinders/m^2. This produced a frontal area per unit volume of $a = nd$, and a solid volume fraction of $\phi = n\pi d^2/4$ within the patch. Upstream of the patch, the velocity is uniform with magnitude U_o (Fig. 1). As flow approaches the patch, the velocity begins to decelerate about 1D upstream, as flow is diverted around this region of high drag. Diversion and flow deceleration continue through the patch. While the mean velocity within the patch is diminished relative to the free stream, the turbulence levels may be enhanced, as turbulent eddies form in the wake of each individual cylinder.

Because the patch is porous, some flow penetrates through the patch, creating an area of slow streamwise velocity directly behind the patch, which we call the steady wake region. The presence of flow in the steady wake delays the onset of the von Kármán vortex street and thus alters the wake structure relative to that observed behind a solid obstruction (Nicolle and Eames, 2011; Zong and Nepf, 2012). The flow in the steady wake (U_1) separates two regions of faster velocity (U_2), creating a shear layer on either side of the steady wake. These layers grow linearly with distance from the patch, eventually meeting at the wake centerline (Fig. 1). At this point, the interaction between the shear layers results in the von Kármán vortex street. The length L_1 between the end of the patch and the onset of the von Kármán vortex street defines the length of the steady wake region (Ball et al., 1996). The length of the steady wake region (L_1) may be predicted from the growth of the linear shear layers and the patch geometry (Zong and Nepf, 2011),

$$L_1 = 2.5D\frac{(1+U_1/U_2)}{(1-U_1/U_2)} \approx 2.5D\frac{(1+U_1/U_o)}{(1-U_1/U_o)} \quad (1)$$

The right most expression assumes $U_2 = U_o$, which is reasonable if D is much less than the channel width, which is valid in our experiments.

The formation of the von Kármán vortex street provides a lateral flux of momentum that erodes the velocity deficit in the wake. After the additional distance L_2, the velocity profile again approaches the upstream value, U_o. The region L_2 is called the wake recovery region. Based on data given in Zong and Nepf (2012), we propose the following empirical relation:

$$\frac{L_2}{D} = 13\frac{U_1}{U_o} + 4 \quad (2)$$

The total length of the wake is $L_1 + L_2$.

For a solid cylinder, the von Kármán vortex street begins immediately behind the obstruction, so that $L_1 = 0$, and $L_2/D \approx 3$ ($Re_D = 23000$; Zong and Nepf, 2012). Behind a porous obstruction, L_1 and L_2 increase with increasing steady wake velocity, U_1 (Eqs. (1) and (2)). Because U_1 increases with increasing patch porosity (i.e. decreasing ϕ), L_1 and L_2 increase with decreasing ϕ. Because these length scales describe important features of the flow field, i.e., the onset of the von Kármán vortex street (L_1) and the end of the wake velocity deficit ($L_1 + L_2$), we hypothesize that they can be connected to the pattern of erosion and deposition observed near a patch. This hypothesis will be tested in the current study.

Bedload transport is characterized by the bed shear stress,

$$\tau = \rho u_*^2 \quad (3)$$

with ρ the fluid velocity and u_* the bed shear velocity. When the bed shear stress exceeds a critical value (τ_c), sediment motion is initiated; and for conditions of $\tau > \tau_c$, sediment motion increases monotonically with increasing τ (e.g., Julien, 1998). Bed shear stress is known to increase with velocity, but it may also be elevated by turbulent motions (Diplas et al., 2008). From the flow description given above, we expect increased bed shear stress, and therefore increased sediment movement, along the sides of the patch and within the von Kármán vortex street. Because small-scale turbulence may also be generated within the patch, scour is also possible within the patch. Alternatively, we expect bedload accumulation in regions of reduced bed shear stress, specifically in the steady wake region of length L_1, where both velocity and turbulence are diminished.

While we anticipate that a finite patch of vegetation will change bedload transport locally (described above), at the reach scale we expect that the introduction of an isolated patch of vegetation will have little impact. This is because a finite patch alters the flow field over a limited distance (L), beginning about D upstream of the patch and extending downstream a distance $L_1 + L_2$ (i.e., $L = 2D + L_1 + L_2$). Beyond this distance, the flow—and therefore the bedload transport—should be unaffected by the patch. This idea will be tested experimentally by considering the change in net deposition integrated over the length scale L. Note, this length scale should be slightly extended to reflect the saltation distance (L_s). Once a particle is set in motion, it travels (on average) over a length scale $L_s = 150d_s$ (Habersack, 2001). For typical sand grain sizes, this length scale is on the order of 10 cm.

The scour and deposition associated with a circular patch of vegetation will be compared to that observed for a solid cylinder. Dargahi (1990) investigated scour and deposition around an emergent circular cylinder of diameter D = 0.15 m, in a flow of 20-cm depth and 26 cm/s, which are comparable to the flow conditions used here. We use D to denote diameter to allow comparisons to patches of diameter D. Dargahi observed scour beginning 25 s after the initiation of the experiment. The scour hole was roughly circular, extending 1.5*D* upstream from the leading edge and 2*D* downstream from the trailing edge of the cylinder. The sediment scoured from around the cylinder was deposited in a mound that extended to nearly 6*D* downstream from the back of the cylinder. The lateral motion associated with the von Kármán vortex street carried sediment toward the wake centerline so that the deposition mound was on the wake centerline. The volume of scour balanced the volume of deposition so that at the reach scale no net change in sediment volume occurred, which is consistent with the argument presented for finite vegetation patches given in the previous paragraph.

2. Materials and methods

Experiments were conducted at the St. Anthony Falls Laboratory (SAFL; Minneapolis, MN) in a 5-m-long, 1.2-m-wide sediment flume that was filled with an 8-cm layer of Silurian pool filter sand (U.S. Silica, Frederick, MD). The upstream sediment level did not change during the experiment, indicating that the sediment was not supply limited. The median sand grain diameter was 500 μm, and the density was 2.65 g/cm^3. The flume was fed by water drawn from the Mississippi River and controlled by a manual valve. A weir located at the downstream end of the flume was adjusted to achieve the desired flow depth. Circular patches were constructed from cylindrical wooden rods (d = 0.64 cm) placed in a perforated plastic board. Patches were constructed with the following diameters and solid volume fractions: (D = 10 cm, ϕ = 0.1), (D = 22 cm, ϕ = 0.1), and (D = 22 cm, ϕ = 0.03). The maximum patch diameter, D, was 0.18 of the channel width so that the walls have little influence on the flow near the patch. Using a rigid stem model simplifies construction, and it is justified because we focus on conditions with emergent vegetation—for which the flow response is largely two-dimensional, with the flow diversion and the dominant shear layers in the horizontal plane. As long as the plants remain emergent, the magnitude of diversion and lateral shear is set by the nondimensional flow blockage (aD). While a flexible stem might allow flow blockage to change with flow speed, for a given flow blockage, the flow structure in the wake will be the same (Chen et al., 2012). Finally, the basal region of most real stems is rigid, so that our model correctly captures the stem geometry close to the bed (Leonard and Luther, 1995; Leonard and Reed, 2002).

Velocity upstream of the patch was measured with a Nortek Vectrino. The Vectrino was secured to a bar placed on top of the flume, and it was unclamped and moved along the bar to measure different locations across the flume. At the start of each run, the flow rate was manually adjusted until the velocity measured 5 cm below the water surface reached a preselected target velocity (20, 30, or 40 cm/s). A vertical velocity profile was then measured upstream of the patch and 1 m from the inlet flow straightener. Velocity was recorded at each point for 240 s at a sampling rate of 25 Hz. The vertical profile of time-averaged velocity was depth-averaged to obtain the upstream velocity U_o. A lateral transect of velocity was also taken upstream of the patch to confirm the lateral uniformity of the flow profile. Behind the patch, a measurement of U_1 (Fig. 1) was made using a handheld SonTek FlowTracker sampling at 10 Hz over a 30-s interval. Velocity was measured at 0.2 and 0.8 times the water depth. The mean of these values is an estimate for the depth-averaged velocity.

Because we were not able to make velocity measurements within the patch, the turbulence associated with stem generation was estimated using a relation developed and experimentally verified by Tanino and Nepf (2008):

$$k_t = u^2 \left[\frac{\phi}{(1-\phi)\pi/2}\right]^{2/3} \approx U_o^2 (nd^2/2)^{2/3} \qquad (4)$$

where $k_t \equiv (\overline{u'^2} + \overline{v'^2} + \overline{w'^2})/2$ is the turbulent kinetic energy per fluid mass. The right-most expression assumes $\phi << 1$ and substitutes $\phi = n\pi d^2/4$ to explicitly show the relationship with stem density, *n*. Further, because we were not able to measure velocity inside the patch, we substitute $u = U_o$. With this approximation Eq. (4) cannot predict the absolute magnitude of turbulence within the patch but can still serve as a comparative metric between patches. Finally, Eq. (4) is strictly valid only for stem Reynolds numbers $Re_d = ud/\nu > 100$, the limit above which shedding of vortices from the stems is present.

The bed friction velocity, $u_* = \sqrt{\tau/\rho}$, was estimated from a logarithmic profile, assuming smooth turbulent conditions (Julien, 1998),

$$\frac{U_o}{u_*} = 5.75 log\left(\frac{u_* h}{\nu}\right) + 3.25 \qquad (5)$$

where *h* is the water depth, and ν is the kinematic viscosity of water. This profile is valid for $Re_* = \frac{u_* d_s}{\nu} < 4$. Our Re_* values ranged from 2.6 to 9.3, which technically fall in the transition regime. However, estimates of shear velocity were similar (within 5%) using the rough turbulent (Re_* > 70) and smooth turbulent profiles.

The change in bed elevation was found by differencing bed elevation before and after exposure to flow. A Keyence LK-G laser, mounted on a motorized track above the flume, measured the distance to the sediment bed every 2 mm across the flume and every 5 mm along the flume (parallel to the flow field). Before each run, the sand was smoothed with a 1-m-long rigid plastic board, and sediment inside the patch was manually smoothed in order to provide similar initial conditions for each run. The sediment was scanned before and after several hours of flow. The scans were interpolated and plotted in Matlab using code written by Craig Hill (University of Minnesota, Minneapolis, MN). In order to remove very large values associated with individual rods, cells with distances $<$ 700 mm from the laser or with gradients $>$ 0.6 mm/mm were removed; replacement values were interpolated from surrounding cells. Scans taken before and after each run were differenced to find the net deposition as a function of x (streamwise) and y (lateral). Longitudinal transects of laterally averaged deposition were constructed by summing across each lateral (y) scan.

In order to find the net deposition within the patch, the patch center was located using an uncorrected scan, which showed the dowel rods; a circle was defined using the patch center and known radius. Values of net deposition inside the circle were summed in order to find the total net deposition volume within the patch. Net deposition behind the patch was defined as the net deposition within a square of side length D centered directly behind the patch. Uncertainty in the net deposition within and directly behind the patch was estimated by shifting the circle or square by 1 cm in each coordinate direction.

The net deposition at the reach scale was estimated from the average change in sediment height over the area covered by the laser scan. In cases where scour extended upstream of the laser scan, we extrapolated the laterally averaged deposition upstream to the point of zero net deposition. This extrapolation is consistent with the shape of upstream scour holes measured within the laser scan limits and the scour holes measured by Dargahi (1990). For some cases (4, 5, and 10), the net deposition extended downstream beyond the footprint of the scan (an example is discussed in the results section). In these cases, we extrapolated the laterally averaged net deposition from the end of the laser scan to a point of zero deposition at $L_1 + L_2$. This was justified because visual observations confirmed that the patch-induced bedform extended behind the patch approximately $L_1 + L_2$, as anticipated in Section 1. Uncertainty in the channel average net deposition (±1.1 mm) was estimated by comparing two sets of replicates. The variation between replicates was in part caused by the deposition of fine particles, which were present in the Mississippi River water. The concentration of suspended particles varied from day to day, based on observed water clarity. Fine particle deposition was readily apparent from the contrast between the dark brown fine particles and the light tan of the Silurian pool filter sand.

The length of the steady wake, L_1, was estimated using dye, following a method similar to that of Zong and Nepf (2012). Red dye was injected near the surface directly behind the patch, and movies were taken of the dye motion. The point at which von Kármán oscillations were first observed marked the end of the steady wake region. After this evaluation, the flow was left to run for several hours. We chose run times that allowed us to replicate the distinct patterns of erosion and deposition at different flow velocities—2 hours for 40 cm/s velocity, 5 hours for 30 cm/s velocity, and overnight for 20 cm/s velocity. These run times are consistent with Dargahi (1990) who, for comparable flow speeds and depths, observed intense scouring for 3 hours, with 60% of the final scour depth reached after 2 hours. After each run, the flow was stopped and the flume allowed to drain. Excess water was bailed; the remaining water was aspirated, or sucked out of the flume using a hose. Once dry, a laser scan was run on the sediment formation; pictures of the sediment and apparatus were taken.

3. Results

3.1. Flow field

Because it was not feasible to make longitudinal transects of velocity in the SAFL flume, we utilized the detailed transects measured by Zong and Nepf (2012). To do so, we first confirmed that our measured values of U_1 were consistent with those of Zong. Although Zong considered U_o = 10 cm/s and the SAFL experiments consider a range of U_o (10 to 33 cm/s), the flow distribution is expected to be self-similar, i.e., for the same ϕ and D, U/U_o will be the same. This is confirmed in Fig. 2, which shows the longitudinal transects (U/U_o, x/D) made by Zong for D = 22 cm, ϕ = 0.1 and ϕ = 0.03, along with the value of U_1/U_o measured in the SAFL experiments. The SAFL points represent the mean U_1/U_o ratio, and the error bar denotes the standard deviation for all measurements at a given patch geometry (D, ϕ). For both transects, the SAFL values overlap with the detailed profiles of Zong. For the patch D = 10 cm, ϕ = 0.1, we measured U_1/U_o = 0.25 ±0.13, compared to Zong's U_1/U_o = 0.22 ±0.02 (data not shown). Furthermore, our values of L_1 are consistent with the model prediction (Eq. (1)) and with measurements from previous studies (Fig. 3). Given these confirmations, we are confident in using Eqs. (1) and (2) to predict L_1 and L_2, respectively, when these length scales could not be measured directly (Table 1).

The adjustment of flow near the patch depends on the degree of flow blockage provided by the patch, which is described by the patch width, D, and the frontal area within the patch, a. Together, these define a dimensionless flow blockage parameter, aD. The flow diversion and velocity reduction within the patch increase as aD increases. For example, in Fig. 2 the velocity is reduced to a greater extent for the patch with higher aD, specifically ϕ = 0.1, aD = 4.4. In addition, for this case the velocity becomes negative at the end of the steady wake region (about x/D = 3), indicating the presence of a recirculation zone similar to that observed behind a solid body. No recirculation exists behind the sparser patch (ϕ = 0.03, aD = 1.3). A recirculation zone is only present for patches aD > 4 (Chen et al., 2012). Consistent with this, the smaller dense patch (D = 10 cm, ϕ = 0.1, aD = 2.0) does not have a recirculation zone. Later we will see that the presence of the recirculation zone leaves a specific signature in the sediment pattern.

3.2. Solid cylinder

The expected pattern of scour and deposition around a solid cylinder (Dargahi, 1990; Simpson, 2001) was observed in the SAFL flume for a cylinder of diameter *D* = 3 cm (Fig. 4). Unfortunately, we did not capture a laser scan for the initially flat bed, so estimates of net deposition are not possible; however, regions of scour (blue) and deposition (red) are still clearly evident. The white circle indicates the position of the cylinder, and flow occurred from left to right. A circular scour hole is centered on the obstruction with a diameter of 3.5*D*; the deposition mound is located on the wake centerline, extending to about 7*D*. Both observations are consistent with Dargahi (1990), discussed in Section 1. The maximum deposition is located at about 4.8*D*. The scour hole has a maximum depth of 3.4 cm (about 1*D*). The pattern of scour and deposition observed for the solid cylinder is contrasted below with the patterns observed for porous patches.

3.3. Porous patch

The scour and deposition observed for four porous patch experiments are shown in Fig. 5. In the colored contour plots, the upstream (x/D = -1) and downstream (x/D = 0) limits of the patch are marked with black vertical lines. Flow was in the positive *x* direction. The corresponding, laterally averaged deposition is shown next to each contour plot. The wake length scales L_1 and L_2, defined by Eqs. (1) and (2), are shown within the plot—except for case 17, for which the length scales were too far downstream ($L_1 + L_2$ = 615 cm).

We first discuss cases 4 and 5, which represent patches with high flow blockage (*D* = 22 cm, ϕ = 0.1, aD = 4.4; Figs. 5A and 5B). Although these two cases have different channel velocity, U_o = 33 cm/s (case 4) and 17 cm/s (case 5), the patterns of deposition and erosion are similar, which is consistent with the fact that the spatial pattern of the flow is similar, as set by the flow blockage. The sediment pattern for these two cases differs in several ways from that observed with a solid object. First, unlike the circular scour region observed around the solid cylinder (Fig. 4), the scour near the porous patch (blue color) has a horseshoe shape, with deposition replacing scour directly downstream of the patch. The flow passing through the patch (U_1) delivers sediment that is subsequently deposited directly downstream of the patch (red mound just past $x/D = 0$). Second, unlike the solid object (Fig. 4), scour extends very little upstream of the porous patches. This is based on visual observation not captured in the scans. Looking at the laterally averaged transect, we see that in each case scour began at the front of the patch, increased with distance inside the patch for about 0.5D, and then began decreasing. Third, there exist two distinct regions of deposition: the first mound directly downstream ($x/D \approx 0.2$) and a second mound distributed over some distance downstream, but with a peak at $x/D \approx 5$. The position of the second peak in deposition is similar to that observed for the single deposition mound observed behind a solid cylinder (at $x/D = 4.8$; Fig. 4). Notably, the second region of deposition falls on the wake centerline, similar to the solid cylinder; this is again attributed to the lateral transport provided by the von Kármán vortex street. Indeed, the second region of deposition occurs just after the onset of this vortex street, i.e., $x > L_1$ (Figure 5A,B; cases 4 and 5). Some aspects of the dense patch deposition will show similarity with the solid cylinder because, as flow blockage increases, the wake structure approaches that of a solid cylinder. Numerical studies done by Nicolle and Eames (2011) suggested that this occurs for aD >≈ 9. Beyond this limit the wake structure, and likely the deposition pattern, will be identical to that of a solid object.

Perhaps the most striking feature in the wake of this high flow blockage patch is the triangular ridge that grows from the bar of sediment behind the patch (Figs. 5A,B; x/D = 0.25 to x/D = 2.4). The tip of this triangle is located just before L_1 and corresponds to the position at which the recirculation zone occurs at the end of the steady wake (Fig. 2). As noted above, a recirculation zone is present only for cases with $aD \geq 4$. The region inside the triangle did not experience any sand accumulation or depletion. Saltation was observed along the raised border of the triangle but not inside the region, suggesting that bedload transport did not occur inside this region. However, fine particle deposition from the mean flow was observed, as indicated by the contrast between the dark fine particles and lighter color of the Silurian pool filter sand in a photograph (Fig. 6).

For these patches (aD = 4.4), the wake length defined by $L_1 + L_2$ is a good measure of the length of the bed formation associated with the patch. This is visually demonstrated in the panoramic photograph of case 5 (Fig. 6). Near the position marked $L_1 + L_2$, the relatively smooth mound of wake deposition ends; the sediment pattern returns to spanwise ripples, similar to that observed upstream of the patch. From the above discussion, we suggest that for $aD > 4$, the wake length scales L_1 and L_2 can describe key features in the deposition and erosion pattern.

Next, we consider case 17 (Fig. 5C), which was the sparsest patch we considered and the lowest flow blockage (ϕ = 0.03, D = 22 cm, aD = 1.3). Compared to a high flow blockage experiment with comparable D, h, and U_o (case 4, Fig. 5A), the pattern of deposition and erosion has several differences. First, because the changes in the velocity are less pronounced and occur more gradually over space (Fig. 2), the resulting sediment pattern is more diffuse—i.e., the features are less sharply delineated. For example, the scour around the edge of the patch is less pronounced because the flow diversion is less severe (Fig. 5, cases 4 and 17). Second, the mound of deposition directly behind the patch ($0 < x/D < 1$) is larger. This is discussed further below. Third, deposition beyond the first mound ($x/D > 1$) does not occur on the wake centerline but creates a formation that is open to the downstream direction. This open formation is consistent with the absence of a recirculation zone and with the very large value of L_1, which is beyond the end of the image shown. Recall that the von Kármán vortex street provides the mechanism for sediment transport toward the wake centerline, but this mechanism is only present for $x > L_1$. The absence of this lateral transport mechanism near the patch results in deposition that is offset from the centerline, as seen in case 17. We conclude that open formations (e.g., case 17) are favored with low flow blockage patches that produce long regions of steady wake, and closed formations (e.g. case 5) are favored with high flow blockage patches.

Although $L_1 + L_2$ was estimated to be much longer for case 17 than for cases 4 and 5, the length of the sediment formation was similar (Fig. 5). Specifically, in case 5, $L_1 + L_2 \approx 8D$; this length is consistent with the length of the sediment formation (Fig. 6). By contrast, for the sparse case 17, the length of the sediment formation is 4.5*D* (Fig. 5); $L_1 + L_2 = 25D$, a large disparity, suggesting that the wake length is not a good measure of the sediment pattern for sparse patches. When the wake is very long, as in case 17, the sediment supply provided by erosion near the patch likely runs out before the end of the wake is reached.

We next consider case 10 (Fig. 5D), for which $D = 10$ cm, $\phi = 0.1$, $aD = 2$. Because $aD < 4$, no recirculation zone is present in the steady wake zone. Consistent with this, this patch does not generate the closed triangular ridge observed in the high flow blockage cases (e.g., cases 4 and 5 in Figs. 5A,B). However, similar to cases 4 and 5, net deposition along the centerline of the wake begins near L_1 (Fig. 5D). Taken together, the four cases shown in Fig. 5 suggest the following generalization: if sediment supply is sufficient, the onset of the von Kármán vortex street at L_1 produces lateral transport toward the wake center and net deposition on the wake centerline beginning near L_1 (cases 4, 5, and 10, Figs. 5A,B,D). For sparse patches with very large L_1, the sediment scoured from around the patch deposits long before the onset of the von Kármán vortex street, and the absence of significant lateral transport within the steady wake leads to downstream deposition that is displaced from the wake centerline (case 17, Fig. 5C).

The distinctive restructuring of the bed shown in Fig. 5 was not observed in every case. If the flow conditions were below the critical value for bedload transport, then no restructuring of the bed could occur. This is also true for the formation of ripples. The bed shear stress, τ, is used to characterize the threshold of sediment motion. From previous literature on bedforms in open channels (Southard, 1991), we expect to find a threshold value (τ_c) above which ripple formation will be observed. In fact, our data suggest this is true, i.e., the same threshold holds for both types of bedform. Specifically, cases for which no ripples were present also have no patch-driven bed formations. The experimental runs fell into three regimes: (1) no ripples and no patch-driven bed forms; (2) no ripples upstream, but ripples triggered by the flow diversion and acceleration around the patch; and (3) ripples and patch-driven bedforms together (e.g. Fig. 6). In regime (3), ripples did not seem to influence the patch-driven formation; no ripples were observed inside the patch. These three regimes are denoted by different symbols in Fig. 7. <insert Fig 7 near here> A distinct transition in regimes occurs near the value $\tau = 0.05$ Pa. Julien (1998, Fig. 7.6) predicted the initiation of sediment motion near $\tau = 0.28 \pm 0.02$ Pa. We are unsure why the observed and predicted thresholds do not match. The addition of stem generated turbulence may play a role, especially within the patch. Further, the diversion of flow enhances the local velocity, which in turn elevates local bed stress above that predicted from U_o. So, local bed stresses are higher than 0.05 Pa at the transition. The data suggest that the critical shear stress is dependent on aD, with a lower transition value occurring for higher aD. This makes sense because, at higher values of aD, more flow is diverted away from the patch, leading to a greater enhancement of velocity outside the patch and a greater local increase in shear rate.

3.4. Within patch scour

In most cases net scour was observed within the patch, and the degree of scour increased with channel velocity (Fig. 8). Note that in our convention scour is negative net deposition, so that a more negative value indicates a greater mean depth of scour within the patch. A linear regression was fit to the low stem density patches (ϕ = 0.03) and the high stem density patches (ϕ = 0.1) individually to emphasize the difference between these cases. For the high stem density patches, the patch diameter did not have a significant impact so, for simplicity, these two classes are lumped together. For the same channel velocity (U_o), deeper scour occurred within the higher density patches (black symbols and black trend line in Fig. 8A) than in the lower density patches (grey symbols and grey trend line in Fig. 8A). This is also evident in the comparison shown in Fig. 5: for the same channel velocity, case 4 (ϕ = 0.1) experienced much deeper in-patch scour than case 17 (ϕ = 0.03). Increased turbulence generation within the dense patches may be responsible for the increased levels of scour. Using the turbulence level estimated from Eq. (4) as the dependent variable, the measured scour for all patch densities falls on similar trend lines (Fig. 8). This suggests that turbulence level is a better predictor of sediment mobility within the patch than local velocity.

Experiments for which in-patch scour was observed also included a mound of sediment deposition directly behind the patch. This mound consisted, at least in part, of sediment scoured from within the patch. The fraction of in-patch erosion contributing to the mound was estimated as the ratio of mound volume to the volume scoured from within the patch. We only considered cases in which the erosion within the patch was non-zero and net deposition occurred behind the patch. Cases 4 and 10 were omitted because the average net deposition behind the patch was negative owing to scour behind the patch along the sides of the mound (Fig. 5A,D). The mound volume to scour volume ratio decreased as the flow blockage, aD, increased (Fig. 9). To explain this trend, we consider the fraction of flow passing through the patch. Integration of lateral profiles (Zong and Nepf, 2012) indicated that 56% of incoming flow continued through the low flow blockage patch (aD = 1.3), while only 19% of incoming flow continued through the high flow blockage patch (aD = 4.4). Because the high flow blockage patch has higher flow diversion, which carries away a fraction of the sediment scoured from within the patch, the sediment available to deposit directly behind the patch is reduced. This explains the smaller fraction of mound volume to in-patch scour. The higher flow diversion associated with the denser patch also leads to a greater acceleration at the patch edge, which is reflected in the greater scour depth at the patch edge. For example, compare cases 4 and 17 in Fig. 5, which have similar channel velocity. For case 4 (aD = 4.4), the scour on the sides of the patch reached a maximum depth of 7.8 cm, while the deepest point of scour for case 17 (aD = 1.3) was 3.5 cm.

3.5. Net deposition at reach scale

Finally, we consider whether the introduction of a finite patch of vegetation promotes net deposition at the reach scale. Recall that for a solid cylinder, over a distance > 10*D*, the net change in sediment volume is zero (Dargahi, 1990); i.e., no change in net deposition exists at the reach scale. The channel average net deposition is shown in Fig. 10. Two dashed lines indicate the replicate uncertainty (±1.1 mm), and any point falling between these lines we consider to be indistinguishable from zero. All but two cases fall within these lines. We can explain case 15, which showed an intrusion of upstream sediment into the laser scan area, probably caused by loosening of the flow straightener upstream, which allowed a stream of relatively fast-moving flow to progress along the side of the flume. In case 5, the predicted $L_1 + L_2$ overestimated the end of the observed patch-driven bedform by about 15 cm (Fig. 6). If we reduce $L_1 + L_2$ by this amount, the channel-scale net deposition is reduced to 1.6 mm. This is still outside the limits for zero net deposition by a margin of 45%. Setting aside this case, the other 16 cases are supportive of the following tentative conclusion. Although significant sediment redistribution is observed, it is spatially contained within the scale of the patch and wake ($L = 2D + L_1 + L_2$), and the introduction of a single patch does not generate net deposition at the reach scale.

4. Discussion

First, let us consider how the vegetation-induced wake may influence the growth pattern for a patch. The bedload transport described in this study and the suspended load deposition observed in this study and experimentally investigated by Tsujimoto (1999) and Chen et al. (2012) suggest that the wake behind a patch of vegetation is a region of elevated fine particle deposition that is also shaded from significant bedload transport. This would likely make the wake a region of nutrient—rich soil that is favorable for new plant growth, so we expect the patch to grow into the region of the steady wake (L_1). Edwards et al. (1999) and Gurnell et al. (2001, 2008) observed a similar patch growth process leading to a mature streamlined formation in the Tagliamento River, Italy. In this case, spring flooding produced an initial deposit of woody debris on a gravel bar. During subsequent low intensity flow, debris was trapped in the patch wake. Gurnell et al. (2001) and Zong and Nepf (2010) also observed a limited area of fine particle deposition upstream of a patch and attributed this to local flow deceleration.

The enhanced flow at the edges of a finite patch (which induced scour in our experiment) would likely inhibit patch growth in the lateral direction. The regions of high bed shear stress created by flow diversion produced areas of scour in sand with d_{50} = 0.5 mm. However, in preliminary tests we considered beds of d_{50} = 1.8 mm. For this larger grain size, no sediment motion occurred around the patches at any of the flow speeds considered. Given this differential in behavior, we anticipated that the diverted flow could selectively transport the finer grains in a graded sediment bed and create an armor layer by leaving only the grains that are too large to be moved by the flow (Carling and Reader, 1982; Jackson and Beschta, 1982; Lisle, 1995**).** Although fine particle deposition in the steady wake has been proposed as the dominant mechanisms by which a pioneer island expands into a streamlined, elongated formation (Tooth and Nanson, 1999; Gurnell et al., 2001, 2008), armoring of island sides may be an additional mechanism, preventing lateral island expansion. Indeed, Edwards et al. (1999) observed scour similar to that observed in our study around islands in the Tagliamento River. Taken together, these processes of deposition and erosion suggest that after a finite patch of vegetation (or woody debris) is introduced, growth of the patch is promoted inline with the patch (mostly downstream, but also upstream); while growth is inhibited in the lateral direction, leading to patches that are elongated in the streamwise direction. Indeed, this is consistent with the shapes observed for instream islands (Gurnell et al., 2001, 2008) and vegetation patches (Sand-Jensen and Madsen, 1992).

Second, the wake behind a patch of vegetation may provide refuge to fish. The wakes of vegetated regions are similar to the wakes of boulders and woody debris in shallow flow, in that the wakes contain regions of low turbulence directly behind the obstruction where wake-scale structures (i.e. the Kármán vortices) are suppressed. For vegetation patches, the Kármán vortices are delayed by the flow through the patch (Zong and Nepf, 2012). In shallow flow conditions, as is typical for boulders, the Kármán vortices are suppressed by the bed friction (Chen and Jirka, 1995; Tritico and Hotchkiss, 2005). Fish prefer these areas of reduced velocity and turbulence because fighting slower currents requires less energy, and these areas often allow fine particle deposition of larvae or macroinvertebrates (Crowder and Diplas, 2000; Roni et al., 2006). Although the literature on fish interaction with vegetation wakes is limited, we suspect that pool-preferring fish will similarly prefer the steady wake zone behind vegetated patches, with the added enticement of prey species activity inside the vegetation patch (Pihl et al., 1994; Collier et al., 1999; Harrison and Harris, 2002). Further, ripples triggered by the patch or areas of scour holes around the patch may provide refuge for small fish (Gerstner, 1998).

Finally, in this study we observed increased scour within the patch with increased stem density. Although this may be somewhat surprising, it is consistent with previous observations. Zong and Nepf (2011) measured flow and fine particle deposition in a long patch of model vegetation. Near the leading edge of the patch, u was close to U_o so that the stem-generated turbulence (Eq. 4) raised the turbulence levels within the patch above that measured in the adjacent open channel. The elevated levels of turbulence suppressed deposition below that measured for an adjacent bare bed. With the scaling argument that follows, we propose that a good fraction of a circular patch behaves like the leading edge of a long patch, with u close to U_o, so that turbulence will be elevated (relative to the bare bed) over a significant fraction of a circular patch. This elevation of turbulence explains the observed scour.

When flow encounters a long patch of vegetation of width D, the velocity in the patch will decelerate in response to the elevated flow resistance provided by the vegetation. This deceleration occurs within the patch over a length scale L_u, which is roughly equal to the larger of D and a^{-1} (Rominger and Nepf, 2011). Because we only consider patches for which $aD \geq 1$, we reasonably anticipate that $L_u \approx D$. This means that the entire patch length is needed to reach the diminished velocity expected within an extended patch of vegetation, and therefore we can assume $u \approx U_o$ within some non-negligible fraction of the patch. This is true for both sparse and dense patches. Together with Eq. (4) and the observations of Zong and Nepf (2011), we expect that the turbulence level within the circular patch will be elevated, relative to the same flow conditions over a bare bed, which explains the observation of scour.

Similar observations of scour within circular patches of vegetation have been observed in the field. Bouma et al. (2007) placed dense (ϕ = 0.02, D = 2 m) and sparse (ϕ = 0.001, D = 2 m) patches of bamboo canes (d = 6-8 mm) in a sandy section of an intertidal flat. They observed higher within-patch erosion for the denser patch. The scour began just before the leading edge of the patch and continued about 0.5D into the patch, after which sediment accumulation was observed. Bouma's pattern is similar to our observations, except that in our cases the maximum sediment accumulation was always behind the patch rather than inside the patch. This difference could be related to the submerged flow conditions that occurred near high tide in the Bouma study, whereas our study considers only emergent flow conditions.

The result that finite length patches of higher stem density experience greater in-patch erosion stands in contrast to observations in long meadows, for which near-bed turbulence is enhanced within sparse meadows but suppressed within dense meadows (see discussion in Nepf, 2012). For a patch whose length is much greater than L_u, most of the patch experiences fully developed flow. For fully developed flow, the velocity within the patch will depend on the stem density, with u decreasing as n increases. Changes in TKE with increasing stem density then reflect the competing effects of reduced velocity and increased turbulence production (Eq. (4)). These opposing tendencies produce a nonlinear response in which the turbulence levels initially increase with increasing stem density, but decrease as n increases further. So, long sparse canopies experience turbulence that is elevated above the bare bed level, but long dense canopies experience turbulence that is diminished below the bare bed level. The enhancement of near-bed turbulence within sparse meadows can lead to the removal of fines, a process called sandification, while the suppression of near-bed turbulence within dense meadows can lead to a preferential accumulation of fines, a process called muddification (van Katwijk et al., 2010). Similarly, Sand-Jensen (1998) investigated the effect of submerged vegetation on flow and sediment composition in streams. Fine particle deposition was observed in patches dense and long enough to display turbulence suppression, while open streamlined canopies had little effect on flow or sediment.

5. Conclusion

Flow around a circular patch of vegetation creates both deposition and erosion in a pattern that can be linked to the mean and turbulent flow field. None of the conditions considered led to sediment accumulation within the patch, and most of the patches had some degree of scouring. Scouring increased with increasing stem density, and this trend can be explained by the expected higher level of turbulent kinetic energy within a finite patch of higher stem density. For the lowest flow blockage (ϕ = 0.03, aD = 1.3), 80 to 100% of the sediment scoured from within the patch was deposited within one patch diameter directly behind the patch. Additional deposition occurred farther downstream but at the sides of the wake, creating an open bed formation (e.g., case 17, Fig. 5). For the highest flow blockage (ϕ = 0.1, aD = 4.4), strong flow diversion carried away much of the sediment scoured from within the patch so that the mound directly behind the patch contained < 50% of this scoured material and as little as 5%. For aD = 4.4 and 2.0, a second region of deposition occurred just beyond L_1, where the action of the von Kármán vortex street directed deposition to the centerline of the wake, creating a closed bed formation (e.g. cases 4, 5, 10, Fig. 5). In all but one case, the redistribution of sediment was contained within the patch and wake length scale $L = 2D + L_1 + L_2$, and over this length scale the patch produced zero net deposition.

Acknowledgements

Research assistance was provided by Lijun Zong, Craig Hill, and Sara Mielke. This work was supported by the STC Program of the National Science Foundation via the National Center for Earth-surface Dynamics under Agreement No. EAR-0120914. This material is based upon work supported by the National Science Foundation under Grant No. EAR 0738352. Any opinions, findings, and conclusions or recommendations expressed in this material are those of the authors and do not necessarily reflect the views of the National Science Foundation.

List of References

Abt, S., Clary, W.P., Thornton, C.L., 1994. Sediment deposition and entrapment in vegetated streambeds. J. Irrigation Drainage Eng. 120 (6), 1098-1111.

Afzalimehr, H., Dey, S., 2009. Influence of bank vegetation and gravel bed on velocity and Reynolds stress distributions. Int. J. Sediment Research 24 (2), 236-246.

Ball, B.J., Stansby, P.K., Alliston, N., 1996. Modeling shallow water flow around pile groups. J. Fluid Mech 351, 167-199.

Bennett, S., Pirim, T., Barkdoll, B., 2002. Using simulated emergent vegetation to alter stream flow direction within a straight experimental channel. Geomorph. 44, 115–126.

Bennett, S., Wu, W., Alonso, C.V., Wang, S.Y., 2008. Modeling fluvial response to in-stream woody vegetation: implications for stream corridor restoration. Earth Surf. Process. Landforms 33, 890-909.

Bouma,T.J., van Duren, L.A., Temmerman, S., Claverie, T., Blanco-Garcia, A., Ysebaert, T., Herman, P.M.J., 2007. Spatial flow and sedimentation patterns within patches of epibenthic structures: combining field, flume and modelling experiments. Cont. Shelf Res. 27 (8), 1020-1045.

Braudrick, C.A., Dietrich, W.E., Leverich, G.T., Sklar, L.S., 2009. Experimental evidence for the conditions necessary to sustain meandering in coarse-bedded rivers. PNAS 106 (40), 16936-16941.

Carling, P.A., Reader, N.A., 1982. Structure, composition and bulk properties of upland stream gravels. Earth Surface Processes and Landforms 7, 349-365.

Chambers, P.A., Prepas, E.E., 1994. Nutrient dynamics in riverbeds - the impact of sewage effluent and aquatic macrophytes. Water Research 28 (2), 453-464.

Chen, D., Jirka, G., 1995. Experimental study of plane turbulent wakes in a shallow water layer. Fluid Dyn. Res. 16, 11-41.

Chen, Z., Ortiz, A., Nepf, H., 2012. Flow and turbulence in the wake of a porous obstruction, and the implications for deposition near a circular patch of emergent vegetati In press WWR.

Collier, K.J., Champion, P.D., Croker, G.F., 1999. Patch- and reach-scale dynamics of a macrophyte-invertebrate system in a New Zealand lowland stream. Hydrobiologia 392, 89-97.

Cotton, J.A., Wharton, G., Bass, J.A.B., Heppell, C.M., Wotton, R.S., 2006. The effects of seasonal changes to in-stream vegetation cover on patterns of flow and accumulation of sediment. Geomorphology 77 (3-4), 320–334.

Crowder, D.W., Diplas, P., 2000. Using two-dimensional hydrodynamic models at scales of ecological importance. J. of Hydr. 230 (3-4), 172-191.

Crowder, D.W., Diplas, P., 2002. Vorticity and circulation: spatial metrics for evaluating flow complexity in stream habitats. Can. J. Fish. Aquat. Sci. 59 (4), 633-645.

Dargahi, B., 1990. Controlling mechanism of local scouring. J. Hydraul. Eng. 116 (10), 1197-1214.

Diplas, P., Dancey, C.L., Celik, A.O., Valyrakis, M., Greer, K., Akat, T., 2008. The role of impulse on the initiation of particle movement under turbulent flow conditions. Science 322, 717-720.

Edwards, P.J., Kolmann, J., Gurnell, A.M., Petts, G.E., Tockner, K., Ward, J.V., 1999. A conceptual model of vegetation dynamics on gravel bars of a large alpine river. Wetlands Ecology and Management 7, 141-153.

Fonseca, M.S., Zieman, J.C., Thayer, G.W., 1983. The role of current velocity in structuring eelgrass (*zostera-marina L.*) meadows. Estuarine Coastal and Shelf Science 17 (4), 367-380.

Gerstner, C.L., 1998. Use of substratum ripples for flow refuging by Atlantic cod, *Gadus morhua*. Environmental Biology of Fishes 53, 455-460.

Gurnell, A.M., Petts, G.E., Hannah, D.M., Smith, B.P.G., Edwards, P.J., Kollmann, J., Ward, J.V., Tockner, K., 2001. Riparian vegetation and island formation along the gravel-bed Fiume Tagliamento, Italy. Earth Surface Processes and Landforms 26, 31-62.

Gurnell, A.M., van Oosterhout, M.P., de Vlieger, B., Goodson, J.M., 2006. Reach-scale interactions between aquatic plants and physical habitat: River Frome, Dorset. River Res. Applic. 22 (6), 1535-1467.

Gurnell, A.M., Blackall, T.D., Petts, G.E., 2008. Characteristics of freshly deposited sand and finer sediments along an island-braided, gravel-bed river: the roles of water, wind, and trees. Geomorphology 99, 254-269.

Habersack, H.M., 2001. Radio-tracking gravel particles in a large braided river in New Zealand: a field test of the stochastic theory of bed load transport proposed by Einstein. Hydrological Processes 15, 377-391.

Harrison, S.S.C., Harris, I.T., 2002. The effects of bankside management on chalk stream invertebrate communities. Freshwater Biology 47, 2233-2245.

Jackson, W.L., Beschta, R.L., 1982. A model of two-phase bedload transport in an Oregon coast range stream. Earth Surface Processes and Landforms 7, 517-527.

Julien, P.Y., 1998. Erosion and Sedimentation. Cambridge University Press, New York, NY.

Kemp, J.L., Harper, D.M., Crosa, G.A., 2000. The habitat-scale ecohydraulics of rivers. Ecological Engineering 16 (1),17-29.

Kouwen, N., Unny, T.E., 1975. Flexible roughness in open channels. J. Hydraul. Div. 101 (NHY1), 194-196.

Larsen, L.G., Harvey, J.W., 2011. Modeling of hydroecological feedbacks predicts distinct classes of landscape pattern, process, and restoration potential in shallow aquatic ecosystems. Geomorphology 126, 279-296.

Lawler, D.M., 2008. Advances in the continuous monitoring of erosion and deposition dynamics: Developments and applications of the new PEEP-3T system. Geomorphology 93 (1-2), 17-39.

Leonard, L.A., Luther, M.E., 1995. Flow hydrodynamics in tidal marsh canopies. Limnology and Oceanography 40 (8), 1474-1484.

Leonard, L.A., Reed, D., 2002. Hydrodynamics and sediment transport through tidal marsh canopies. J. Coast. Res. S136, 459-469.

Li, S.S., Millar, R.G., 2010. A two-dimensional morphodynamic model of gravel-bed river with floodplain vegetation. Earth Surf. Proc. Landforms 36 (2), 190-202.

Lisle, T.E., 1995. Particle size variations between bed load and bed material in natural gravel bed channels. Water Res. Res. 31 (4), 1107-1118.

Lopez, F., Garcia, M., 1998. Open-channel flow through simulated vegetation: suspended sediment transport modeling. Water Res. Res. 34 (9), 2341-2352.

Luna, M.C.M. de M., Parteli, E.J.R., Durán, O., Herrmann, H.J., 2011. Model for the genesis of coastal dune fields with vegetation. Geomorphology 129, 215-224.

Mars, R., Mathew, K., Ho, G.E., 1999. The role of the submergent macrophyte *Triglochin huegelii* in domestic greywater treatment. Ecol. Eng. 12 (1-2), 57-66.

Nepf, H.M., 2012. Flow and transport in regions with aquatic vegetation. Annu. Rev. Fluid Mech. 44, 123-142.

Nicolle, A., Eames, I., 2011. Numerical study of flow through and around a circular array of cylinders. J. Fluid Mech. 679, 1-31.

Pihl, L., Wennhage, H., Nilsson, S., 1994. Fish assemblage structure in relation to macrophytes and filamentous epiphytes in shallow non-tidal rocky- and soft-bottom habitats. Environmental Biology of Fishes 38, 271-288.

Pollen, N., Simon, A., 2005. Estimating the mechanical effects of riparian vegetation on stream bank stability using a fiber bundle model. Water Res. Res. 41 (7), W07025.

Pollen-Bankhead, N., Simon, A. 2010. Hydrologic and hydraulic effects of riparian root networks on streambank stability: Is mechanical root-reinforcement the whole story? Geomorphology 116 (3-4), 353-362.

Rominger, J.T., Nepf, H.M., 2011. Flow adjustment and interior flow associated with a rectangular porous obstruction. Journal of Fluid Mechanics 680, 636-659.

Rominger, J.T., Lightbody, A.F., Nepf, H.M., 2010. Effects of added vegetation on sand bar stability and stream hydrodynamics. J. Hydraul. Eng. 136 (12), 994-1002.

Roni, P., Bennett, T., Morley, S., Pess, G.R., Hanson, K., van Slyke, D., Olmstead, P., 2006. Rehabiliation of bedrock stream channels: The effects of boulder weir placement on aquatic habitat and biota. River Res. Applic. 22, 967-980.

Sand-Jensen, K., 1998. Influence of submerged macrophytes on sediment composition and near-bed flow in lowland streams. Freshwater Biology 39 (4), 663-679.

Sand-Jensen, K., Madsen, T.V., 1992. Patch dynamics of the stream macrophyte, *Callitriche cophocarpa*. Freshwater Biol. 27 (2), 277-282.

Schulz, M., Kozerski, H.P., Pluntke, T., Rinke, K., 2003. The influence of macrophytes on sedimentation and nutrient retention in the lower River Spree (Germany). Water Res. 37 (3), 569-578.

Simpson, R.L., 2001. Junction flows. Annual Review of Fluid Mechanics 33, 415-443.

Southard, J.B., 1991. Experimental determination of bed-form stability. Annu. Rev. Earth Planet. Sci. 19, 423-455.

Tal, M., Paola, C., 2007. Dynamic single-thread channels maintained by the interaction of flow and vegetation. Geological Soc. of America 35 (4), 347-350.

Tanino, Y., Nepf, H.M., 2008. Lateral dispersion in random cylinder arrays at high Reynolds number. J. Fluid Mech. 600, 339-371.

Tooth, S., Nanson, G.C., 1999. Anabranching rivers on the northern plains of arid central Australia. Geomorphology 29 (3-4), 211-233.

Tritico, H.M., Hotchkiss, R.H., 2005. Unobstructed and obstructed turbulent flow in gravel bed rivers. J. Hydraul. Eng. 131 (8), 635-645.

Tsujimoto, T., 1999. Fluvial processes in streams with vegetation. J. Hydraul. Res. 37 (6), 789-803.

van Katwijk, M.M., Bos, A.R., Hermus, D.C.R., Suykerbuyk, W., 2010. Sediment modification by seagrass beds: muddification and sandification induced by plant cover and environmental conditions. Est. Coastal Shelf Sci. 89 (2), 175-181.

Wang, C., Yu, J.Y., Wang, P.F., Guo, P.C., 2009. Flow structure of partly vegetated open-channel flows with eelgrass. Journal of Hydrodynamics 21 (3), 301-307.

Wilcock, R.J., Champion, P.D., Nagels, J.W., Crocker, G.F., 1999. The influence of aquatic macrophytes on the hydraulic and physico-chemical properties of a New Zealand lowland stream. Hydrobiologia 416, 203-214.

Wynn, T.M., Mostaghimi, S., 2006. Effects of riparian vegetation on stream bank subaerial processes in southwestern Virginia, USA. Earth Surf. Proc. Landforms 31 (4), 399-413.

Zong, L., Nepf, H.M., 2010. Flow and deposition in and around a finite patch of vegetation. Geomorphology 116, 363-372.

Zong, L., Nepf, H.M., 2011. Spatial distribution of deposition within a patch of vegetation. Water Res. Res. 47, W03516.

Zong, L., Nepf, H.M., 2012. Vortex development behind a finite porous obstruction in a channel. J. Fluid Mech. 691, 368-391.

Sediment patterns near a model patch of reedy emergent vegetation

Elizabeth M. Follett and Heidi M. Nepf

Table and Figures with Captions

Table 1. Summary of experimental conditions[a]

Expt #	U_o (cm/s)	a (cm^{-1})	ϕ	D (cm)	h (cm)	U_1 (cm/s)	Duration (h)	In-patch scour (cm^3)	Deposit behind patch (cm^3)	L_1 (cm)
1	25	0.20	0.1	22	12	0.4	2	-840±60	420±9	65
2	13	0.20	0.1	22	23	0.7	2	40±11	42±1	>120
3	25	0.20	0.1	22	12	0.4	2	-83±18	21±2	70
4	33	0.20	0.1	22	13	2.8	2	-2475±2	-200±20	58
5	17	0.20	0.1	22	9	1.3	23	-1450±60	29±12	52
6	20	0.06	0.03	22	9	--	23	-490±20	704±12	>120
7	24	0.06	0.03	22	12	--	5	-660±20	830±20	>120
8	16	0.06	0.03	22	24	--	23	24±1	42±0.3	>120
9	21	0.06	0.03	22	26	1.3	5	14±2	19±1	>120
10	32	0.20	0.1	10	13	1.3	2	-565±6	-209±13	42
11	26	0.20	0.1	10	14	0.9	2	-269±12	150±10	31
12	20	0.20	0.1	10	11	4.2	5	-266±12	139±9	34
13	15	0.20	0.1	10	9	3.1	19	-60±70	41±3	36
14	17	0.20	0.1	10	9	1.4	4.25	-274±13	153±7	33
15	19	0.06	0.03	22	13	18	4.25	-1110±20	860±20	>120
16	10	0.20	0.1	22	23	0.9	19	-39±2	62±2	36
17	30	0.06	0.03	22	12	21	2	-1228±12	940±30	>120
±	0.5			0.5	0.5	0.5				2

[a]Depth-averaged velocity U_o (m/s), frontal area per unit volume a (cm^{-1}), solid volume fraction ϕ, patch diameter D (cm), flow depth h (cm), flow in the steady wake zone behind the patch U_1, duration of flow (hours), in-patch scour (cm^3), direct deposit behind patch in a square of side length D centered directly behind the patch (cm^3), and L_1 (cm) estimated from dye injections. In several cases L_1 was greater than 120 cm, the end of the visual zone; for these cases, L_1 is denoted >120. U_1 was not measured for experiments 6-8. Uncertainty given in last row.

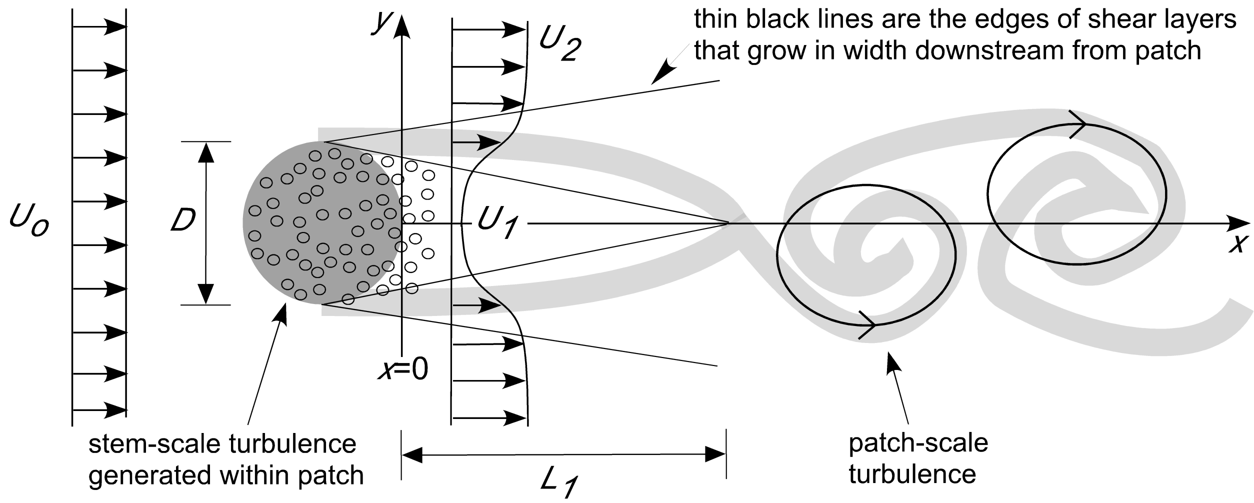

Fig. 1. Schematic diagram of wake behind a porous circular patch showing upstream velocity (U_o), steady wake velocity (U_1), velocity outside the wake (U_2), and the length of the steady wake region (L_1). Stem-scale turbulence shown by small black circles within and just behind the patch. Light grey lines represent tracer released at the two sides of the patch. The tracer reveals the eventual onset on the von Kármán vortex street.

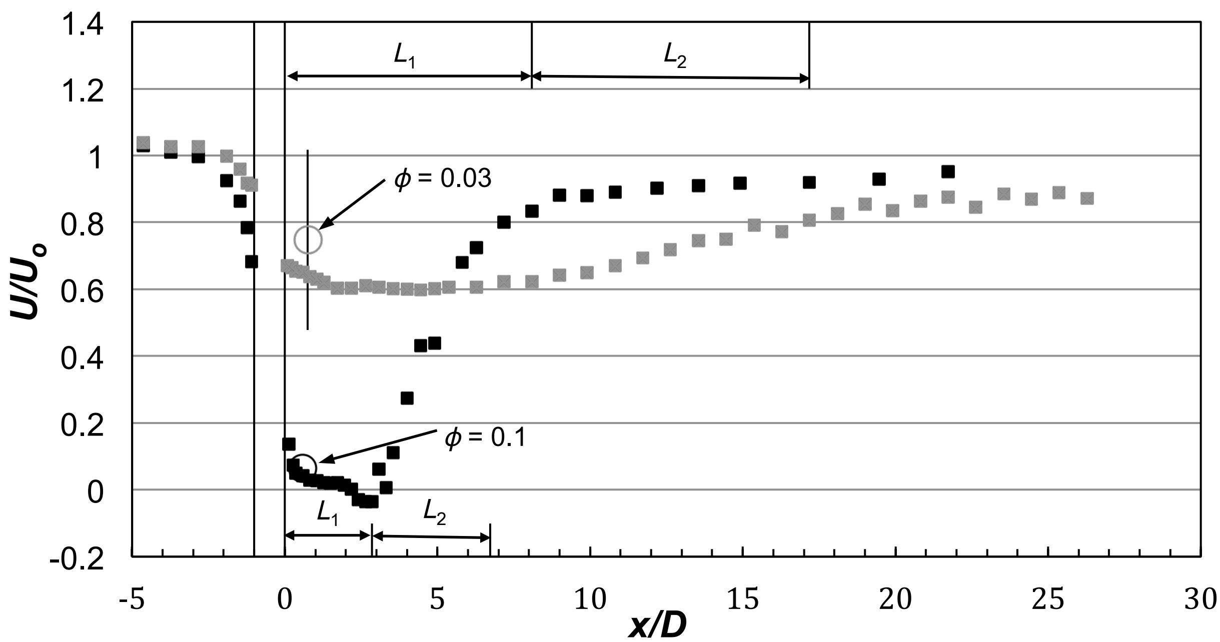

Fig. 2. Plot of U/U_o vs. x/D for a patch of diameter D = 22 cm. Patch is located between x/D = -1 and 0. L_1 and L_2 are plotted for reference. Profiles measured by Zong and Nepf (2012) shown by small squares: ϕ = 0.1, aD = 4.4 (grey squares) and for ϕ = 0.03, aD = 1.3 (black squares). Our measurements are shown by open circles in grey (ϕ = 0.03, aD =1.3) and black (ϕ = 0.1, aD = 4.4). The vertical bar on our points corresponds to the standard deviation among all cases with the same aD.

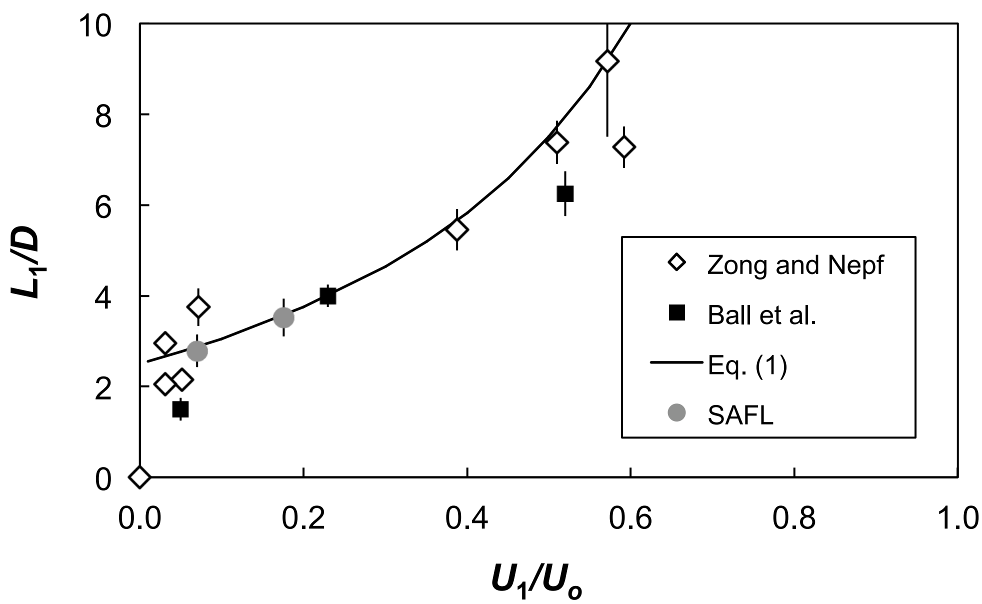

Fig. 3. L_1/D vs. U_1/U_o. L_1 is measured by dye injection. Model Eq. (1) is shown as a solid line.

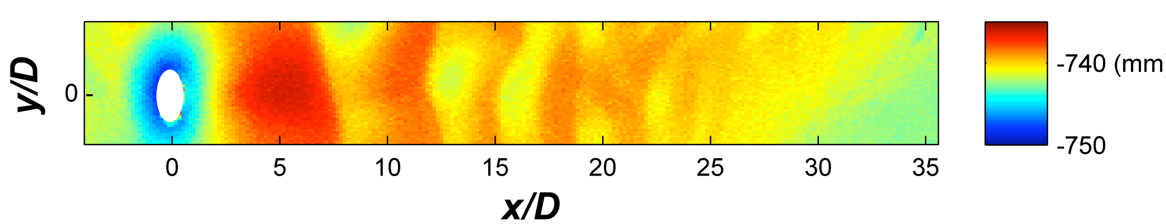

Fig. 4. Laser scan of sediment formation around solid cylinder of diameter *D*=3 cm. The white oval indicates the position of the cylinder; the y coordinate has been stretched. Because a laser scan was not taken prior to this experiment, the sediment is not zeroed. Units are mm from the laser probe.

(a)

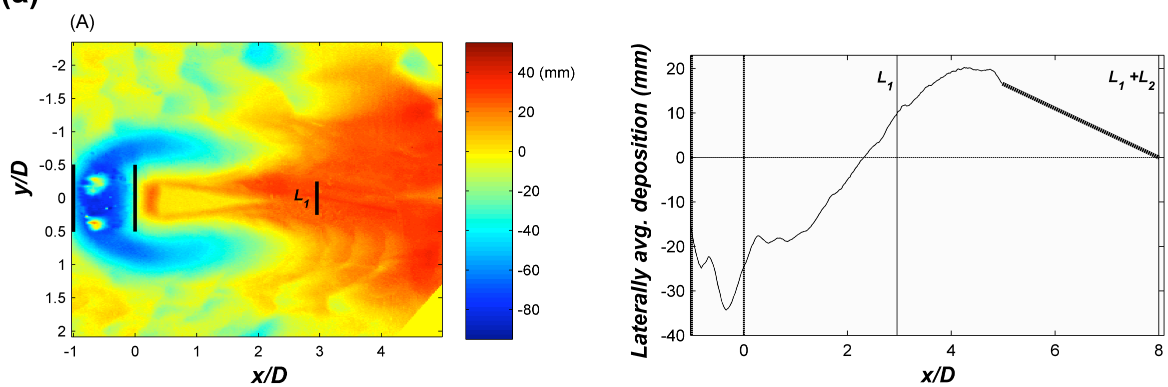

(b)

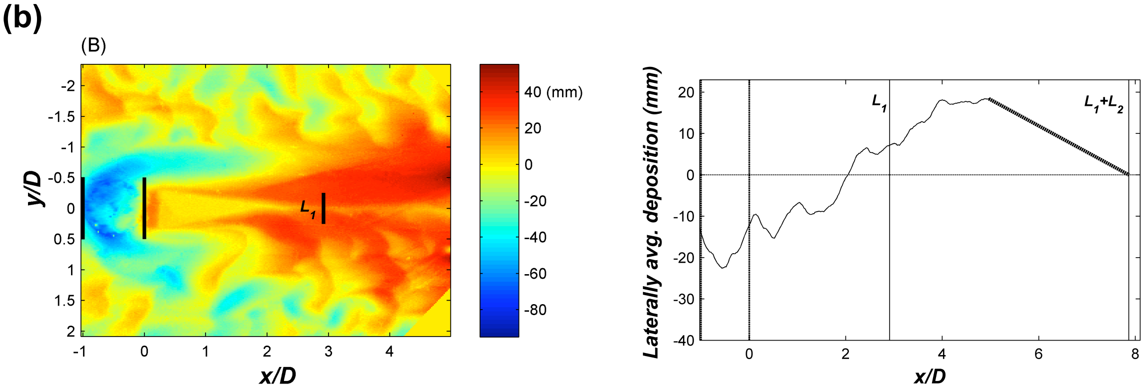

(c)

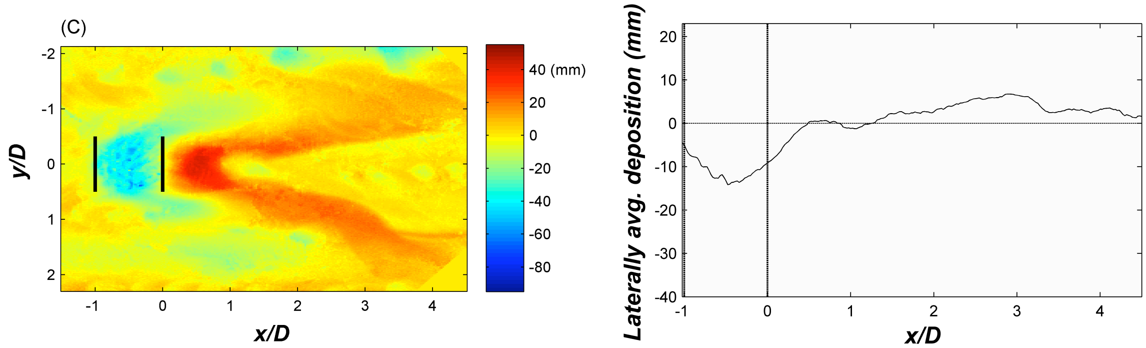

(d)

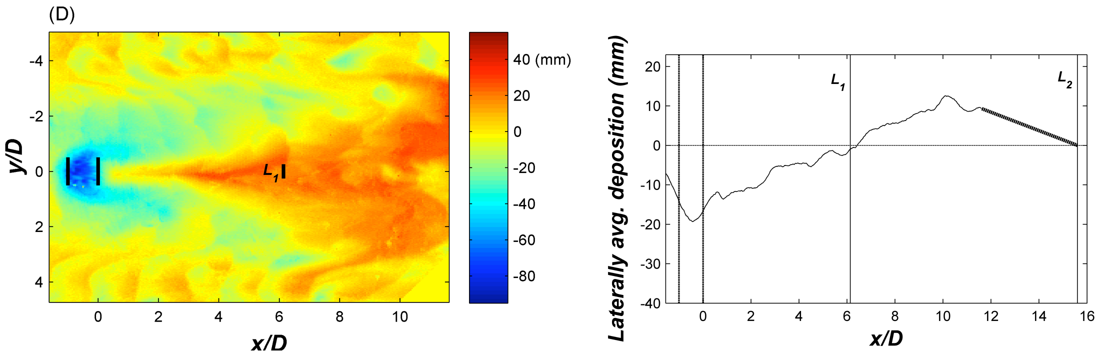

Fig. 5. Net deposition estimated from laser scans. Yellow indicates zero net deposition; red and orange indicate positive net deposition; blue and green indicate negative net deposition (scour). Longitudinal (*x*/*D*) profiles of laterally averaged net deposition are located next to each laser scan. The patch is located between *x*/*D*= -1 and 0, noted by vertical dashed lines in the laterally averaged profiles. **(A)** case 4: ϕ = 0.1, *D* = 22 cm, U_o = 0.33 m/s, aD = 4.4; **(B)** case 5: ϕ = 0.1, *D* = 22 cm, U_o = 0.17 m/s, aD = 4.4; **(C)** case 17: ϕ = 0.03, *D* = 22 cm, U_o = 0.30 m/s, aD = 1.3; **(D)** case 10: ϕ = 0.1, *D* = 10 cm, U_o = 0.32 m/s, aD = 2.0. Heavyweight dashed lines represent the extrapolation out to L_1 + L_2.

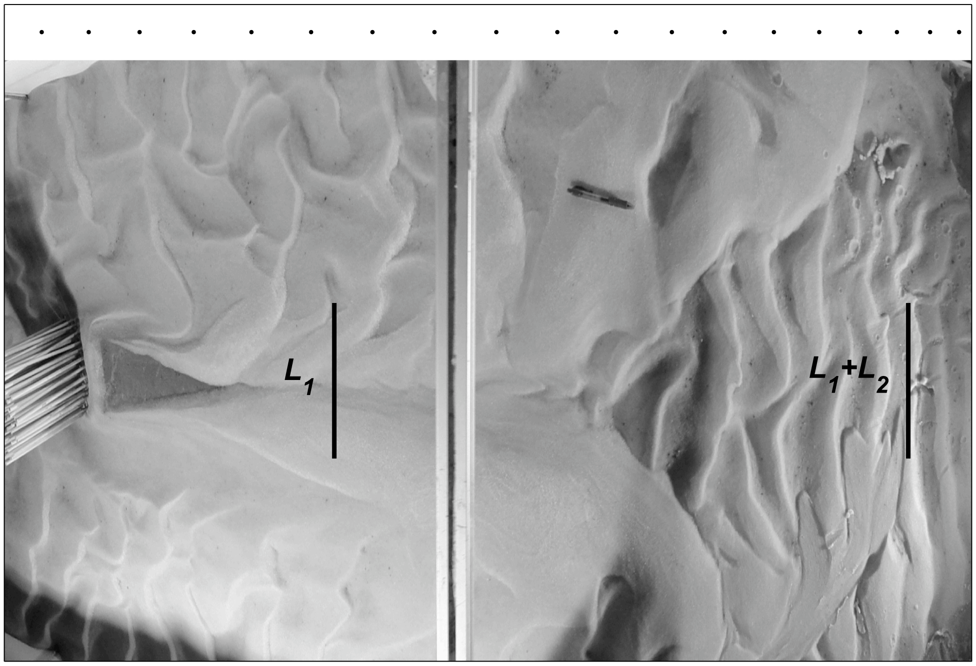

Fig. 6. Panoramic photograph of case 5 (D = 22 cm, ϕ = 0.1, U_o = 0.17 m/s). The darker triangular region directly behind the path indicates fine particle deposition. Markers above picture indicate one decimeter of real space, and the first marker is located at x = 10 cm. x = 0 is the downstream edge of the patch. L_1 and L_2 are marked for reference.

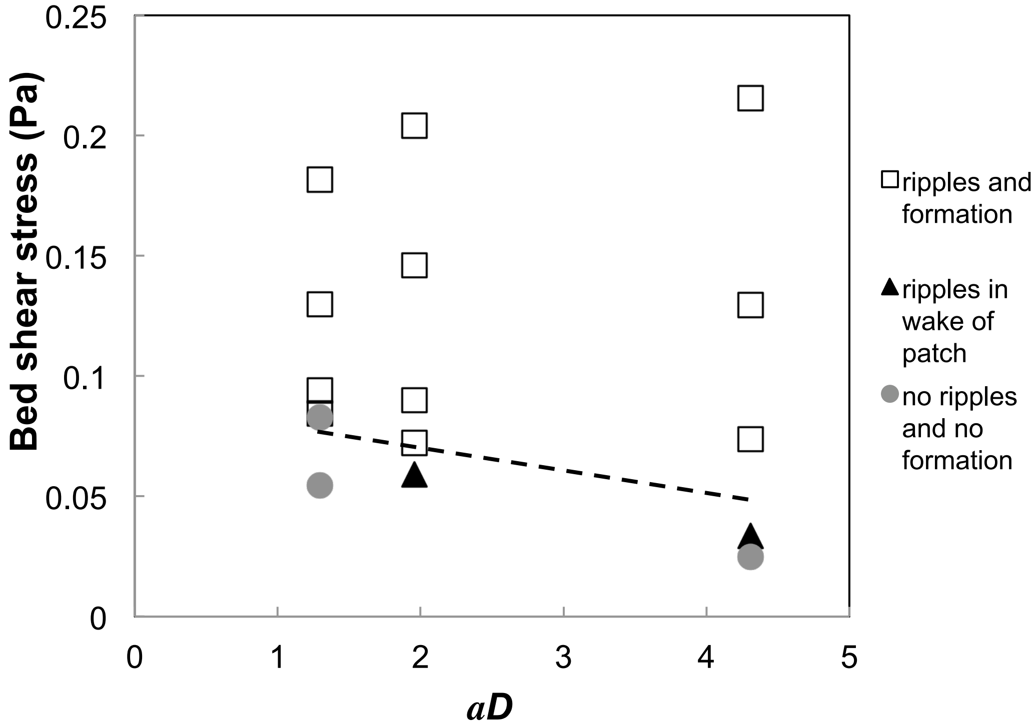

Fig. 7. Classification of cases by bed shear stress (Pa). Ripples and patch-induced formations were not observed for flow conditions with low shear stress but were observed for high bed shear stress. For conditions with intermediate values, ripples were only observed in the patch wake. Error is contained within the symbols. Dashed line represents bed stress transition from conditions that do (above line) and do not (below line) lead to sediment formations.

(a)

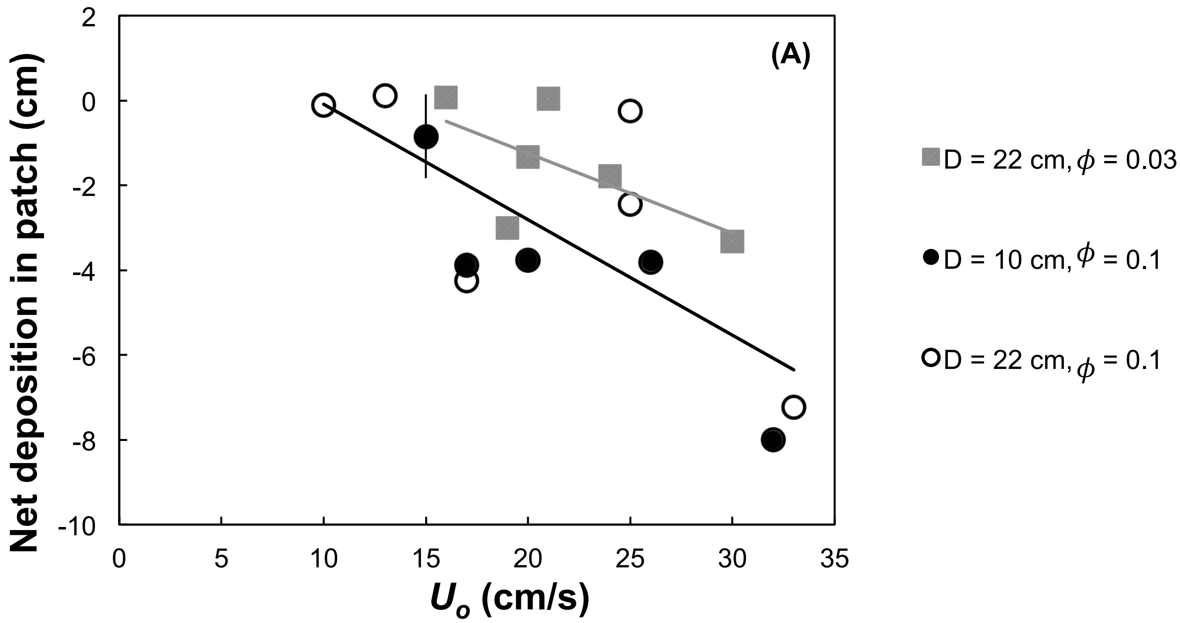

(b)

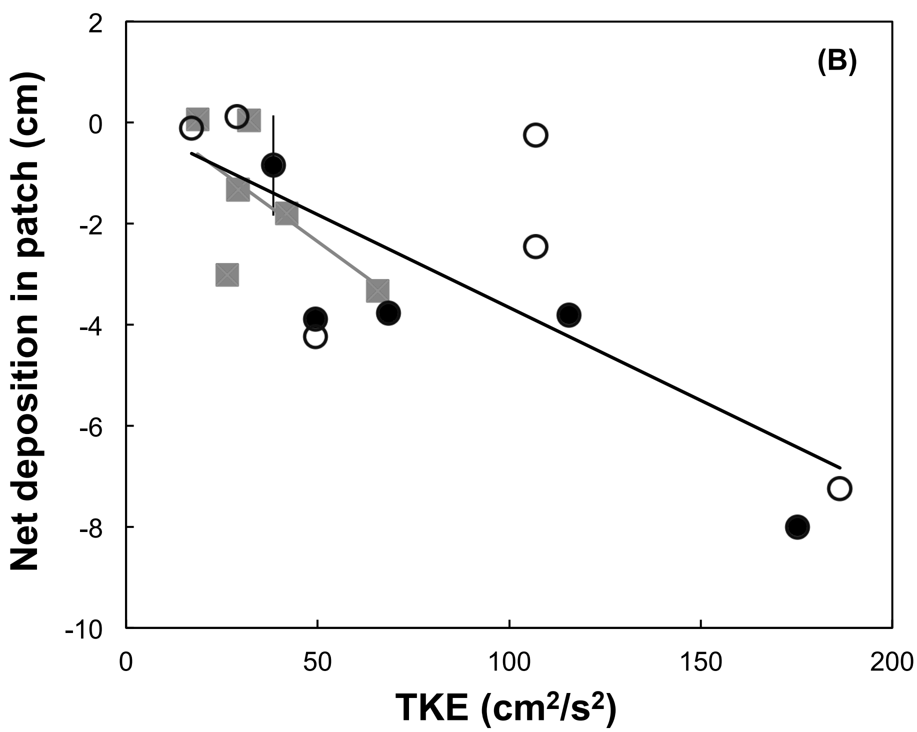

Fig. 8. Net deposition within the patch (cm) versus **(A)** depth average upstream velocity U_o (cm/s) and **(B)** turbulent kinetic energy TKE (cm^2/s^2) estimated from Eq. 4. Black

lines show linear trends among ϕ = 0.1 cases; gray lines show linear trends among ϕ = 0.03 cases. In most cases, error bars were within the marker size.

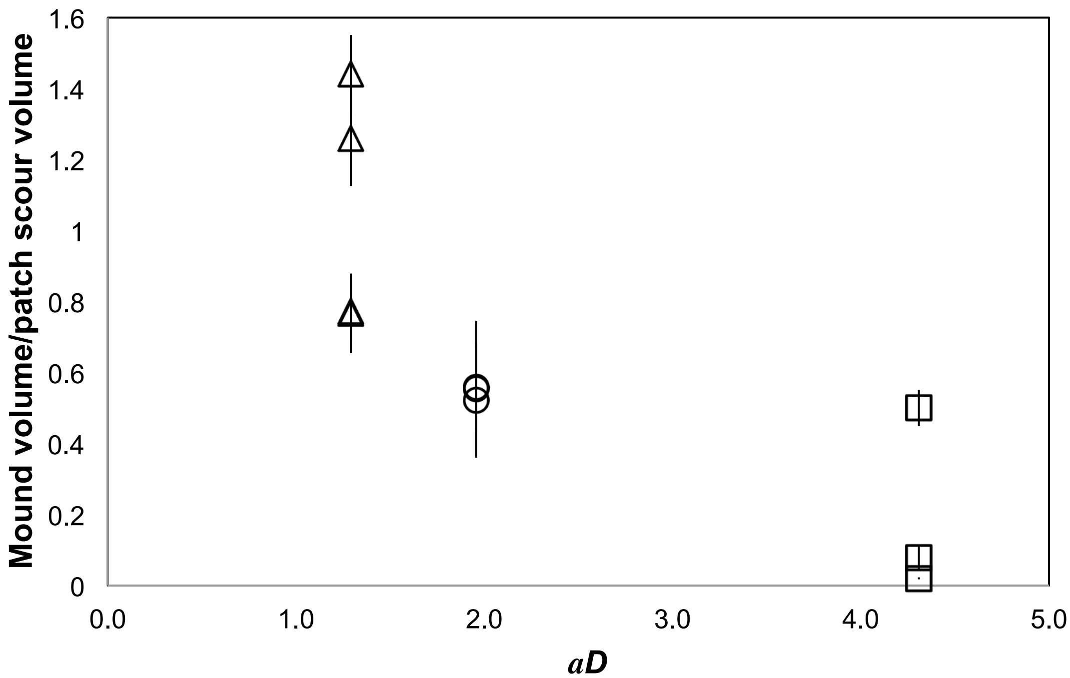

Fig. 9. Ratio of mound volume behind the patch to scour volume within the patch. Mound volume was defined as the volume of sediment deposited in a square area of side length *D* centered directly behind the patch. △: ϕ = 0.03, *D* = 22 cm; ○: ϕ = 0.1, *D* = 10 cm; □: ϕ = 0.1, *D* = 22 cm.

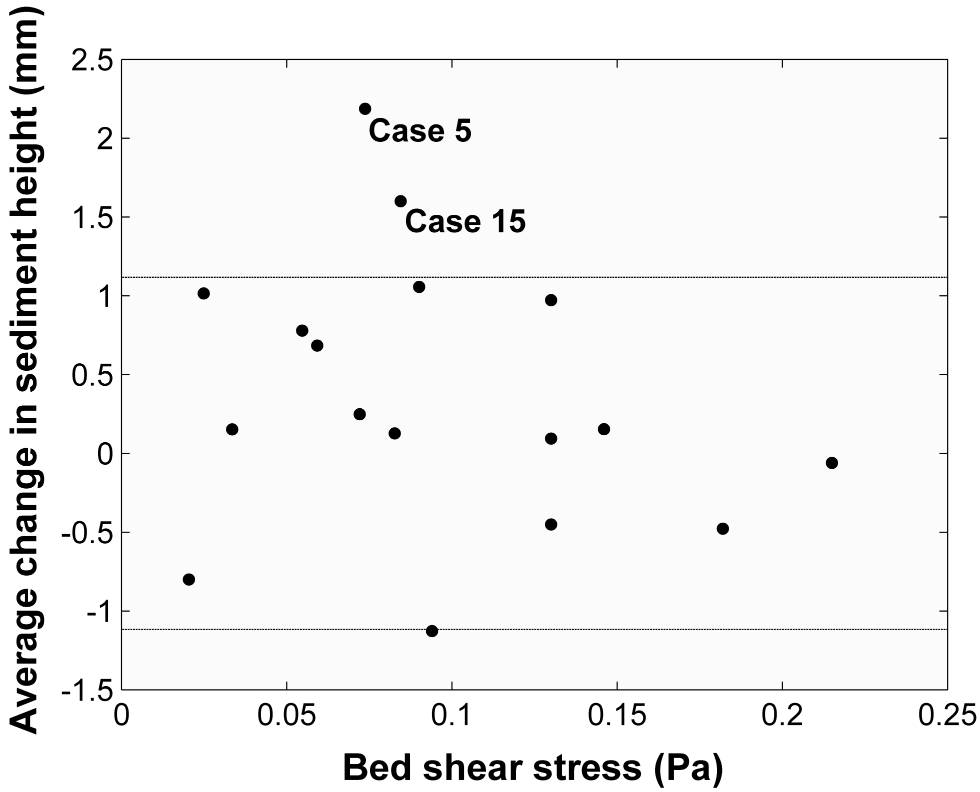

Fig. 10. Average change in sediment height (mm) vs. bed shear stress (Pa) at the reach scale. Variability between ±1.1 mm (dashed line) represents the estimated uncertainty based on the observations of two sets of replicates.